UNCONVENTIONAL RESOURCES TECHNOLOGY CONFERENCE
FUELED BY SPE • AAPG • SEG

URTeC: 2691531

The plug drum effect, or why your microseismic events may not be where you think they are

Guillaume Bergery*, Total SA, France; Zhishuai Zhang, University of California, Berkeley; Jing Du, Total E&P R&T, Houston; D. Diller, T. Shuck, B. Fish, NanoSeis.

Summary

Microseismic is the only 3D real time monitoring tool and is therefore commonly used during hydraulic fracture operations to provide an insight into the generated fracture pattern. It has expanded rapidly in recent years due to the development of unconventional plays. An accurate velocity model is required to accurately locate microseismic events. An initial velocity model is usually built using a sonic log, and then calibrated using perforation shots with known locations. The calibration process involves identifying P-waves and/or S-waves generated by the perforation shots. In this paper we will show examples of perforation data acquired from surface and from borehole arrays during fracturing treatment in horizontal wells, and demonstrate the importance of correct identification/classification of the different arrivals in the wave train for calibrating the velocity model. The data examples shows secondary arrivals, right after the direct P-wave arrivals, which have a larger amplitude and a lower frequency compared to the direct P-wave arrivals. Through various analyses these arrivals are identified as compressional waves converted from tube waves after they interact with the plug installed in the wellbore. That is what we call the plug drum effect. An important consideration is that unless the plug drum effect is recognized and handled properly, the velocities and statics (near surface corrections) calibrations will produce incorrect locations for events.

Introduction

The key aspect of microseismic technology in unconventional development is to monitor hydraulic fracture growth and behavior over time, and map the stimulated reservoir volume. This aspect is achieved by installing geophone arrays to passively listen to the P-waves and S-waves waves that are emitted by the slippages on the weakness planes or natural fracture planes induced by the hydraulic fractures. Two main types of acquisitions are used to record the seismicity generated during the fracturing operations: either a large dense array of geophones deployed at surface or more often a string of three component geophones deployed in a nearby observation well. Whatever the acquisition type the processing requires a velocity model in order to locate the microseismic activity. Despite the numerous velocity data usually available - such as check shot VSP, sonic logs, or seismic stack velocities, the velocity model needs to be calibrated using perforation shots to produce accurate microseismic results.

Plug-and-perf completion is the most standard completion technique for unconventional wells, and each perforation shot will provide an active source with a known location in space. These sources are commonly used to calibrate the microseismic velocity model. Prior to the velocity model calibration the positioning error of the perforation shot using the initial velocity model can be as large as several hundreds of feet.

Once the velocity model is calibrated, the microseismic events are located using either traditional earthquake location algorithms (picking-based) or imaging-based algorithms. Velocity plays a key role in obtaining reasonable event locations, achieving good interpretation of the microseismic data, and making sound engineering decisions. During the velocity calibration process, correctly identifying various phase arrivals in the wave train is crucial, as multiple wave arrivals (direct P-wave and S-waves, reflected, converted phases, etc.) have been observed in the perforation data. Depending on the acquisition geometry, velocity structure of the formation, and relative perforation location to the receiver array, certain phases are easier to identify than others.

During the microseismic processing of a horizontal well acquired from a dense array of geophones deployed at surface we realized that all the perforation shots of a same stage were imaging at the exact same horizontal position (same x,y), even though the measured depth of each perforation shot was different. This pattern was observed for every single stage: systematically all the perforation shots of a same stage imaged at the same position and closer to the toe than expected.

By looking carefully at the data in the trace domain, two different wave arrivals were identified only a few tens of milliseconds apart. Surprisingly the second wave arrival had a larger amplitude and a lower frequency content than the first one. The two wave arrivals separation seen on the data corresponds almost exactly to the time it would take for a P-wave to propagate from the perforation location to the plug location in water.

All of the microseismic monitoring projects in this area have similar behavior. This effect is observable for both horizontal and vertical fractured wells, and whether the microseismic array is at the surface or deployed in an observation borehole.

Our interpretation is that when a perforation shot is released, a first wave travels directly in the formation and is recorded at surface. But a wave is also being emitted within the well. This wave travels in the fluid that is filling the well until it reaches the plug. The plug then acts as a second source of emission and will generate a P-wave that will transmit into the formation and be recorded at surface. We call it the plug drum effect and it is represented in Figure 1.

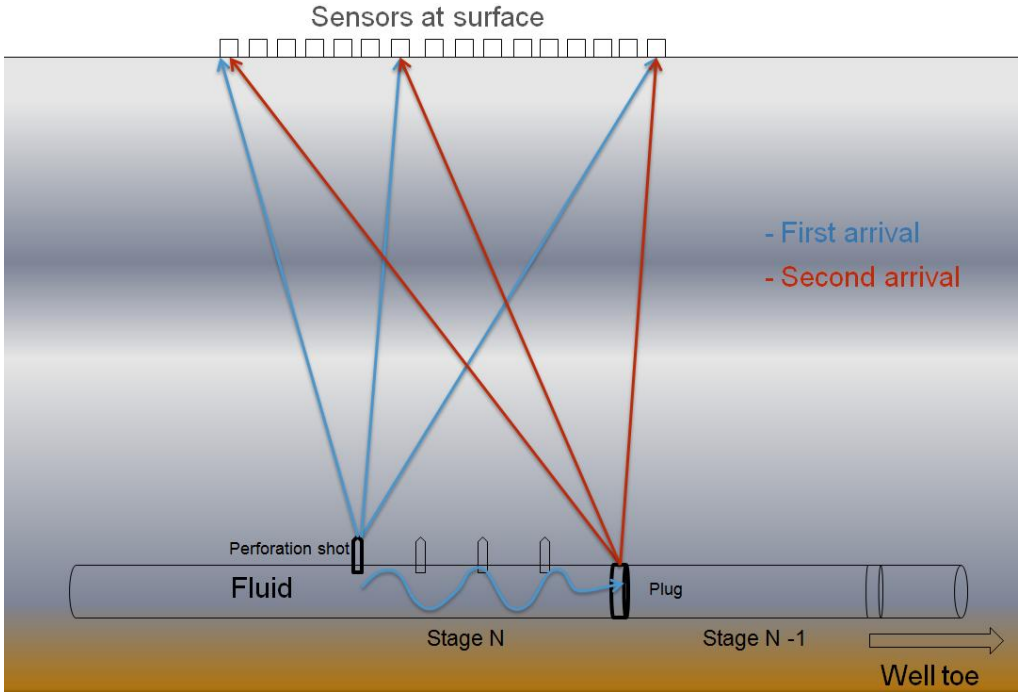

Figure 1: Plug Drum effect schematic - Section view

During the hydraulic fracturing of this horizontal well, a string of geophones was also deployed in a nearby observation well. A secondary arrivals is also observed between the P-wave and S-waves of the perforation data. By considering that this arrival is generated at the plug, it is possible to estimate the plug location from these arrivals. This inferred plug location is consistent with the true plug location. The velocity of the tube wave in the wellbore could also be estimated using the arrival times of this phase and is shown to be a typical tube wave velocity.

At this stage it was interesting to determine if this horizontal well was an exception or the rule, in terms of signal generated when perforated. By reprocessing three horizontal wells and one vertical we concluded that all the wells processed or reprocessed were showing the same behavior.

If this effect is not taken into account during the velocity model calibration, the resulting incorrect velocity and statics models will attempt to relocate the plug at the perforation shot locations. Those incorrect velocities and statics will then be used in subsequent processing to locate all the microseismic events at incorrect locations. The location errors from this problem are likely to be significantly larger than the location errors normally associated with surface microseismic monitoring. For borehole velocity calibration the exact same principle applies. One of the benefits of this finding is that a perforation shot actually generates two distinct sources at known locations that can be used to calibrate the velocity model.

Our interpretation is different from the observations found in the literature. Seher et al. (2014) showed that the secondary arrivals are shear wave converted from tube wave, in this case study both the treatment and observation wells were vertical. Van Renterghem et al. (2015) also studied a case where the late arrivals were present in both surface and borehole data, but arrived later than the direct shear waves.

Surface data example

The example presented here is from a surface acquisition for a hydraulic fracture stage. The surface monitoring network has approximately 25,000 1C surface receivers. The data for two perforation shots are shown in Figure 2. The left two plots are from the 4th perforation shot, and the right two plots are from the 3rd perforation shot for the same stage. In each raw data plot, there are three sub-plots. The left two are sub-stacks along each receiver lines, the plot on the right is the trace data corrected for travel time (equivalent to one-way move-out).

From the top two plots in Figure 2, we can see that the first arrivals are perfectly flattened across the entire receiver array, when using the perforation shot location to perform the travel time correction. Therefore those events imaged at the right perf locations (represented in yellow color). From the two bottom plots in Figure 2 we show that the second arrival are perfectly flattened across the entire receiver array, when using the plug location to perform the travel time correction. Therefore those secondary arrivals imaged at the correct plug locations (represented in yellow color). The same P-wave velocity model is used to correct for the travel time between either the perforation shot location or the plug location and the geophone locations at surface. This also means that the secondary arrivals are compressional waves.

Another significant observation is that the separation between the first and secondary arrivals decreases as the perforation moves closer to the plug location. The separation in the two right plots is smaller than the one in the two left plots. From the time separation and distance between the perf and plug, we computed the tube wave velocity is 1450 m/s.

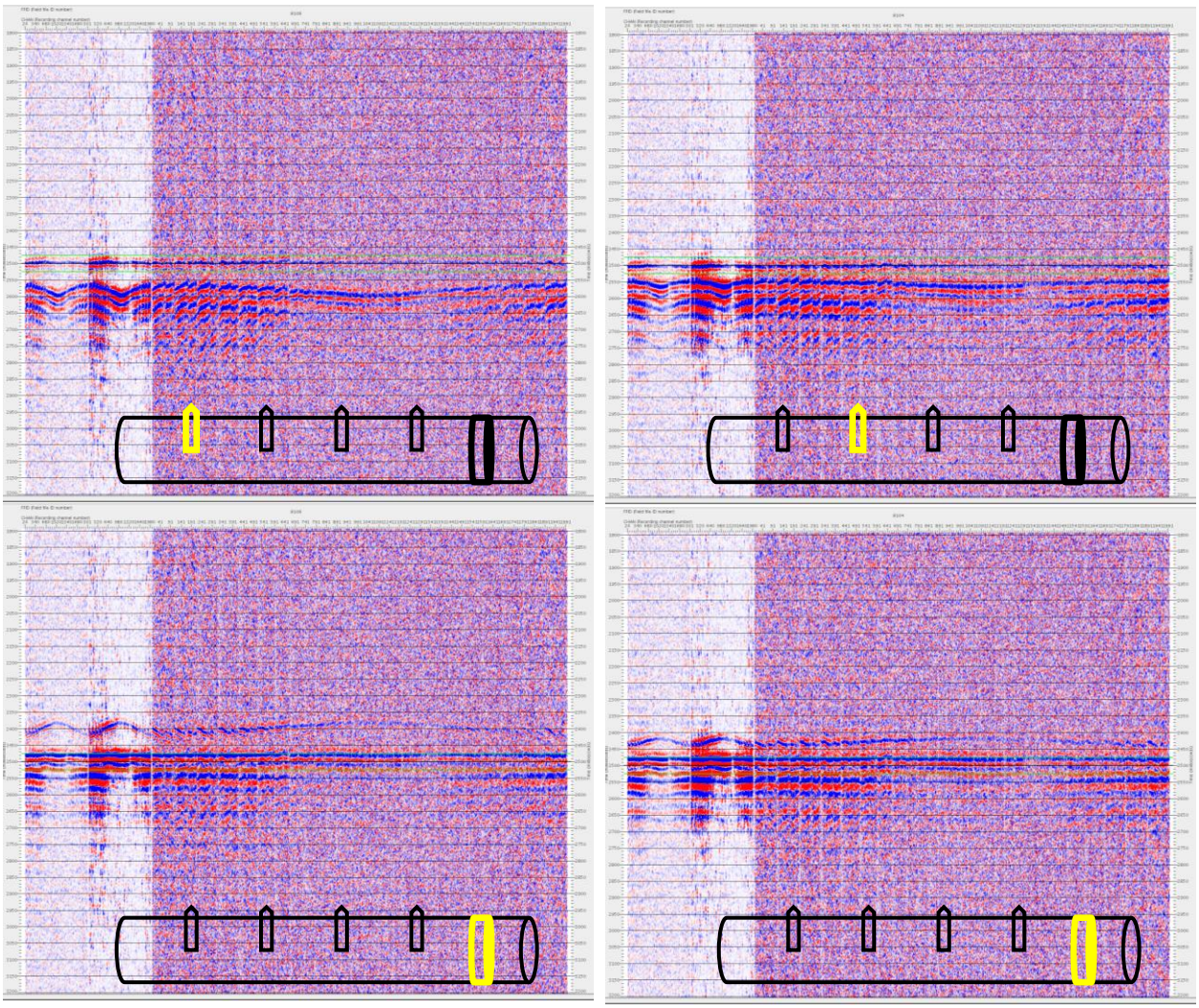

Figure 2: Two surface perforation data examples. The upper images show the traces corrected to the perforation shot locations, and the lower images show the traces corrected to the plug location. The traces are sorted by azimuth, which makes location errors conspicuous.

Downhole data example

The perf drum effect has also been observed in a downhole microseismic survey. We analyzed the microseismic data to verify the existence of the perf-drum effect and study the characters of this phase, which can be useful for its identification in microseismic data analysis.

The hydraulic fracturing acquisition geometry for the downhole survey is shown in Figure 3. The horizontal stimulation well was drilled perpendicular to the expected fracture azimuth in the target formation and completed as a cemented lateral using a plug-and-perf. The microseismic data was acquired by a 24-tool, 12-level double-stacked receiver array positioned in the adjacent vertical observation well. In this paper we look at the three perforation shots recorded in Stage 1.

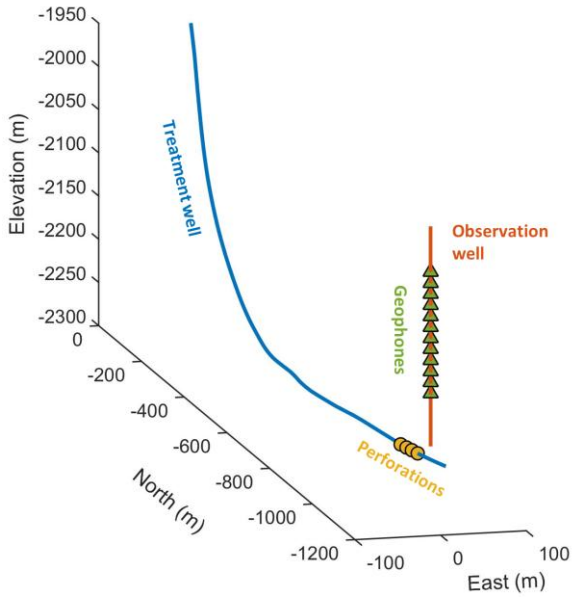

Figure 3: Stimulation project and microseismic survey setup. The borehole array consist a 24-tool, 12-level double-stacked receivers deployed in an adjacent vertical observation well.

Unknown phase between P- and S-wave arrivals

In the waveform generated by perforation shots, we observed an event between the P-wave and S-wave arrivals as indicated by the yellow picks in Figure 4. The amplitude of this phase is comparable to the P-wave, however, it has a lower frequency content. The moveout of this phase is similar with the initial P-wave. Our initial assumption of this phase was a reflection from a high velocity contrast layer interface below the perforation.

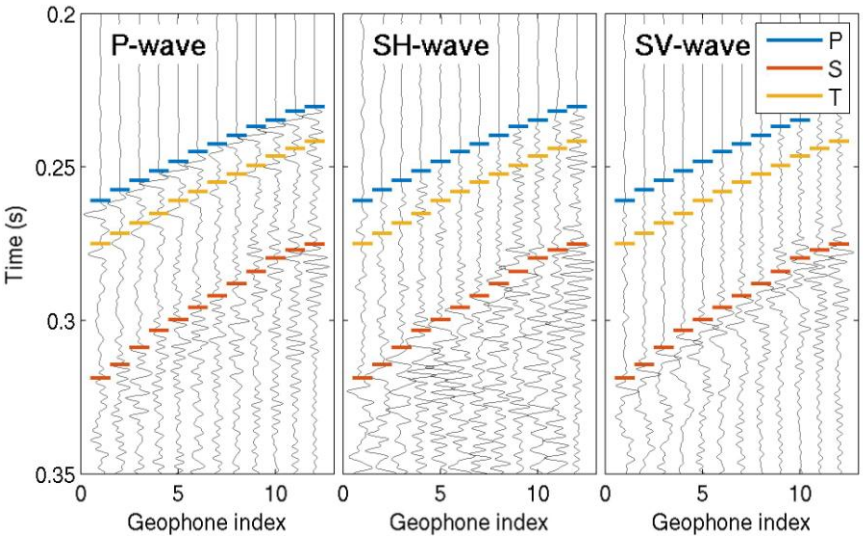

Figure 4: A typical perforation waveform. The T phase indicated by the yellow picks is the phase we studied in this section.

Assumed cause #1: Reflection from lower high velocity layer

The initial assumption for the cause of this phase was a reflection from the high velocity layer at the elevation around -2,305 m (Figure 5). However, we were not able to match the relative arrival times and moveout of these events using ray tracing as shown in Figure 6 to Figure 8. In addition, we can see that as the perforation shot goes further from the geophone array, the travel time difference ($\Delta \boldsymbol{t}$ = Unknown phase arrival time − P-wave arrival

time) between the unknown phase and the P-wave is larger ($\Delta t_{perf2} < \Delta t_{perf3} < \Delta t_{perf4}$, Figure 9). This is contradicted by our ray tracing results, which shows as the perforation shot goes further from the geophone array, the travel time difference between the unknown phase and P-wave should be smaller ($\Delta t_{perf2} > \Delta t_{perf3} > \Delta t_{perf4}$, Figure 9). This contradiction shows that the unknown event between P-wave and S-wave cannot be reflection from the high velocity layer as previously thought.

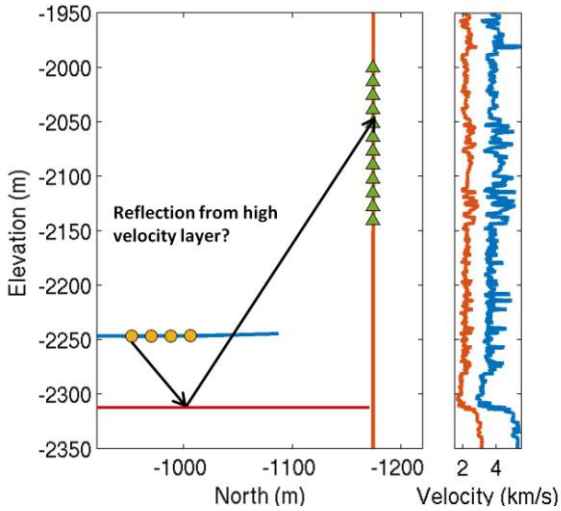

Figure 5: One assumption of the unknown event is due to the reflection from the lower high velocity layer around -2300 m.

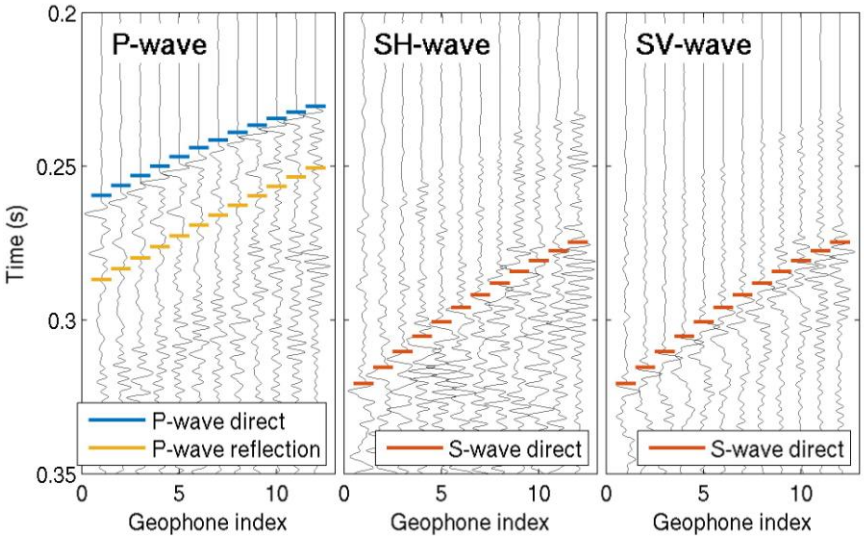

Figure 6: Ray tracing arrival times of perforation shot 2 overprinted on its real waveforms.

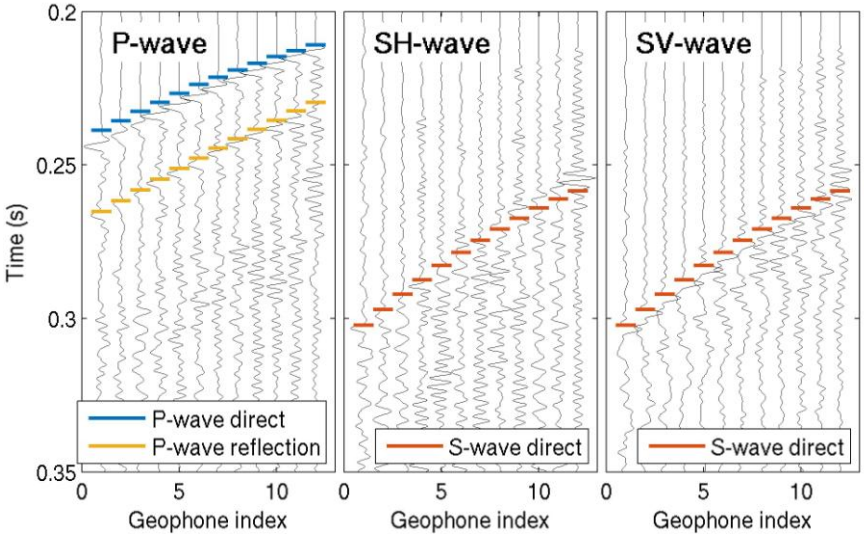

Figure 7: Ray tracing arrival times of perforation shot 3 overprinted on its real waveforms.

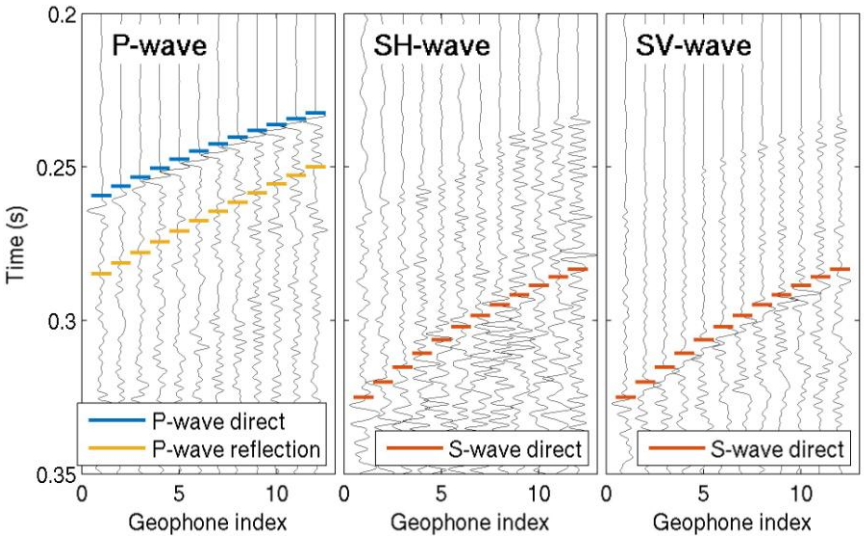

Figure 8: Ray tracing arrival times of perforation shot 4 overprinted on its real waveforms.

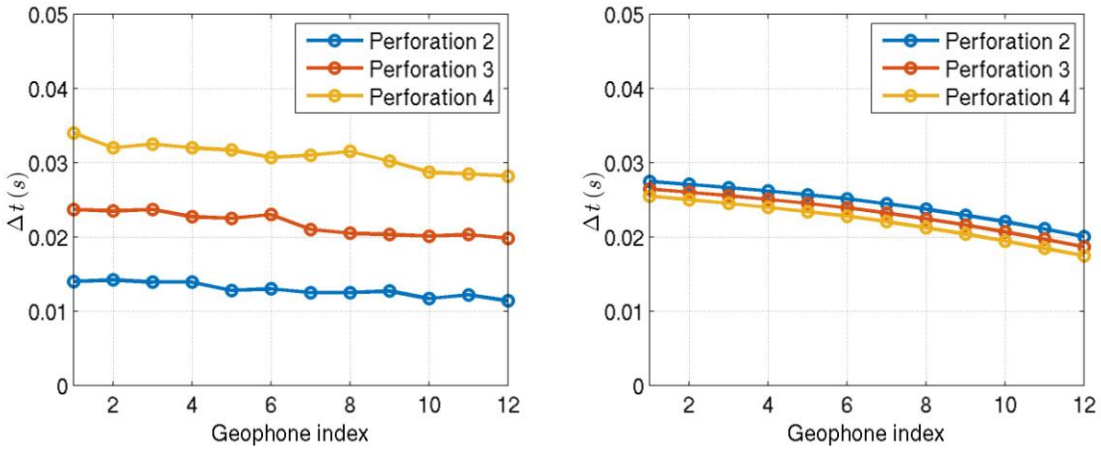

Figure 9: Left: the picked travel time differences between the unknown phase and the P-wave (Δt = Unknown phase arrival time − P-wave arrival time). For the real data, $\Delta t_{\text{perf2}} < \Delta t_{\text{perf3}} < \Delta t_{\text{perf4}}$. Right: the arrival time difference between the reflected P-wave and the direct P-wave (Δt = reflected P-wave arrival time – direct P-wave arrival time). For the ray tracing result, $\Delta t_{\text{perf2}} > \Delta t_{\text{perf3}} > \Delta t_{\text{perf4}}$.

Assumed cause #2: Tube wave generated by perforation shot

Another finding that may help to understand the unknown arrival is that there is a good linear relationship between $\Delta \boldsymbol{t}$ and the measured depth of the perforation shot (Figure 10). From this linear relationship, we can predict that if there is a perforation shot at the measured depth of 3,565 m, the P-wave arrival time will be the same with the unknown phase arrival time. Van Renterghem et al. (2015) have observed tube-wave-to-body-wave conversion in perforation shots in microseismic survey. Our observation suggests that the observed unknown event result from tube wave generated by the perforation shots and emitted out of the wellbore at the measured depth of 3,565 m as shown by Figure 11.

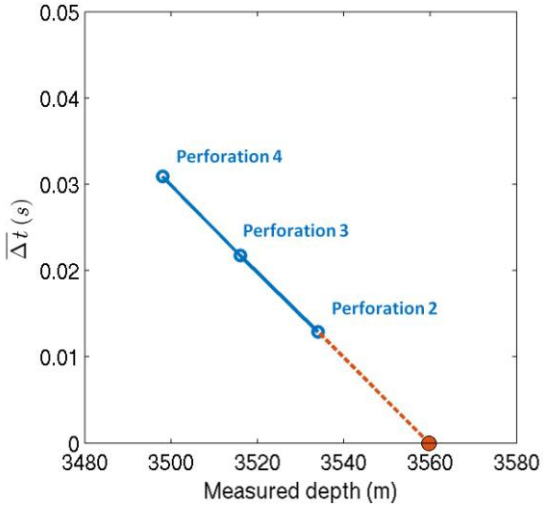

Figure 10: The average time difference between the unknown phase and the P-wave has a linear relationship with the measured depth of perforation shots.

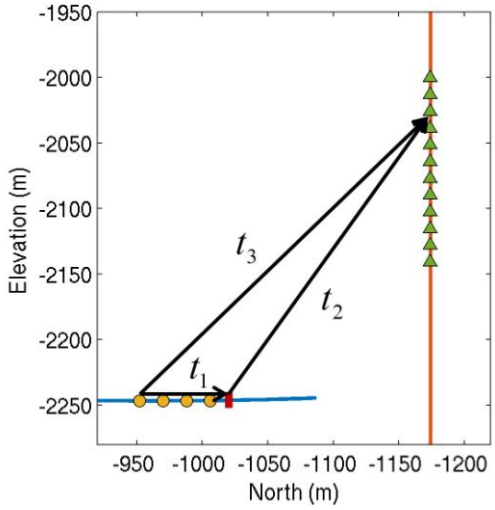

Figure 11: Configuration for the tube wave travel path. From the linear relationship in Figure 16, we can approximate the position where the tube wave emitted out of the wellbore as shown by the red square.

To verify this assumption, we can calculate the wave travel time in the borehole. The various segments of travel times are represented by $\boldsymbol{t_1}$, $\boldsymbol{t_2}$, and $\boldsymbol{t_3}$ as shown in Figure 11. From the relationship, we know:

$$\Delta \boldsymbol{t} = \boldsymbol{t_1} + \boldsymbol{t_2} - \boldsymbol{t_3}, \tag{1}$$

so the travel time of tube wave in the borehole can be obtained by

$$\boldsymbol{t_1} = \Delta \boldsymbol{t} - \boldsymbol{t_2} + \boldsymbol{t_3}, \tag{2}$$

where $\Delta \boldsymbol{t}$ can be calculated from manually pickings of real data, and $\boldsymbol{t_2}$ and $\boldsymbol{t_3}$ can be obtained with ray tracing. The result of each source receiver pair is **shown by** Figure 12**.** From its comparison with Figure 9, where the $\boldsymbol{t}$ value has a dependence on the receiver location, we have successfully corrected for the travel time difference in $\boldsymbol{t_2}$ and $\boldsymbol{t_3}$, and get $\boldsymbol{t_1}$, which is independent of the receiver position. The independence of $\boldsymbol{t_1}$ of the receiver position partially confirms our assumption that the unknown phase is caused by tube waves generated by the perforation shots.

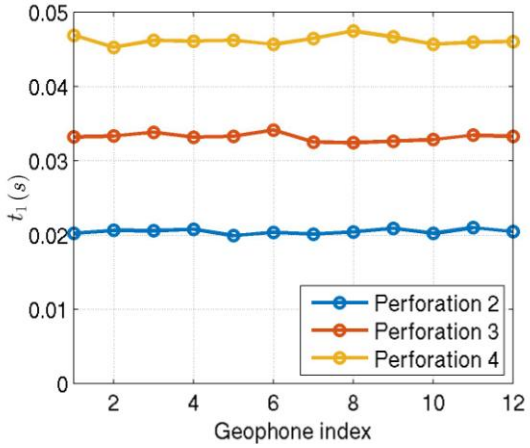

Figure 12: After correcting for the travel time difference in $\boldsymbol{t_2}$ and $\boldsymbol{t_3}$, we get $\boldsymbol{t_1}$, which is independent of the receiver position. This partially confirms the assumption that the unknown phase is caused by tube waves.

We can also calculate the tube wave velocity V_{tube} from t_1 obtained in the previous step:

$$V_{tube} = \frac{MD(perf4) - MD(perf2)}{t_1(perf4) - t_1(perf2)} = 1{,}472\ m/s, \tag{3}$$

where MD stands for the measured depth of each perforation shot. The V_{tube} value of $1{,}472\ m/s$ is a very typical tube wave velocity (Tsang and Rader, 1979; Kurkjian and Chang, 1986; Hsu et al., 1997). This further confirms that the unknown phase we observed results from a tube wave propagation.

With the t_1 value calculated, we can further update the tube wave emission point to be at the measured depth of 3,563 m. After checking this location with the completion diagram, we can find there is a plug at the measured depth of 3,575 m. The interaction between tube wave and the plug may be the cause of the emission body waves out of the wellbore. However, there is a 12 m difference between these two locations. This may be a result of error in deviation survey given the typical large uncertainty in a deviation survey.

Conclusions

In this paper we present the perforation data example recorded in both surface and borehole arrays during hydraulic fracturing treatments. We analyze the later arrivals immediate after the direct P-wave arrivals using various methods such as imaging the secondary arrivals in surface perforation data, examining the separation between the direct arrival and secondary arrival in the surface data, ray tracing for the travel times with reflection, and time delay analysis in the borehole array. The analyses conclude that the secondary arrivals are the compressional waves converted from the tube waves after they interact with plug in the wellbore. With this classification, these additional arrivals could be used along with direct perforation arrivals for velocity calibration, and help avoiding mistakes in velocity building in microseismic monitoring projects.

References

Hsu, C.-J., S. Kostek, and D. L. Johnson, 1997, Tube waves and mandrel modes: Experiment and theory: The Journal of the Acoustical Society of America, **102**, 3277-3289.

Kurkjian, A. L., and S.-K. Chang, 1986, Acoustic multipole sources in fluid-filled boreholes: Geophysics, **51**, 148-163.

Seher, T. S. Rondenay and H. Djikpesse, 2014, Tube wave to shear wave conversion at borehole plugs: Geophysical Prospecting, **62**, 540-551.

Tsang, L., and D. Rader, 1979, Numerical evaluation of the transient acoustic waveform due to a point source in a fluid-filled borehole: Geophysics, **44**, 1706-1720.

Van Renterghem, C., T. Probert, I. Bradford, A. Özbek, and J. O. Robertsson, 2015, A case study revealing the expressions of perforation shots in a shale gas stimulation operation: Geophysics, **80**, WC51-WC60.